Numerical Evaluation of Roughness Influences on Open Water Propeller Characteristics Using RANSE Method

Vu Ngoc Bich
Binh Duong University, Vietnam
Email: vnbich@bdu.edu.vn

Nguyen Thi Ngoc Hoa
Ho Chi Minh City University of Transport, Vietnam
Email: hoa_vt@hcmutrans.edu.vn

***Abstract*—This paper presents the influences of roughness on ship propeller's performance by using RANSE method with moving reference frame approach. The effect of different roughness conditions on the propeller efficiency was evaluated for several different advance coefficients. The numerical obtained results indicate that the thrust of propeller coefficient decreases while the torque of propeller coefficient increases with increasing roughness levels on propeller surface, which leads to a reduction of the propeller open water efficiency. Besides, the paper also investigates into the roughness effect on the pressure, wall skin friction coefficients, and velocity field in order to explain the physical phenomenon of changing propeller characteristics at different roughness levels. The study indicates the proposed RANSE method is capable to apply as a reliable approach to predict the effects of fouling on ship propeller efficiency. The well-known benchmarking Potsdam Propeller was used as test case in this study.**

***Index Terms*—RANSE, propeller, open water, roughness, biofouling, efficiency**

I. INTRODUCTION

During ship operation, the ship wetted surface and its propeller are influenced by the following factors: corrosion; mechanical damages; paint coating damage; accumulation of old paint coating after each reapplication on ship dry dock; barnacle fouling; scratches on the coating surface due to the removal of bio-fouling, poor surface preparation before reapplication… hence, the propeller surface condition becomes rougher than its initial condition (see Fig. 1). This will typically lead to the change of ship resistance and propeller characteristics compared to that of the original ship. As a result, the relationship between ship speed, propeller revolution, and main power is consequently changed.

The influences of fouling on ship drag and propeller performance have been noted, and much of the early studies. The penalty of ship power due to heavy fouling on ship hull could increase as high as 86% [1]. In the same manner, Demirel et al. [2] evaluated the rise in power required for a containership to be 108%, and about 46% for heavy biofouling travelling at 24 knots, and even 10% coverage of 5mm height barnacles respectively. These researches demonstrate that the presence of roughness and biofouling on the ship hull will reduce ship performance.

Currently, there is no complete evaluation method of the roughness and biofouling impact on marine propeller. Therefore, according to [3], it is necessary to develop new approaches or employ the measure data in the evaluation of the impacts of roughness and biofouling on marine propeller characteristics and ship resistance.

Figure 1. Biofouling on ship hull and its propeller during ship operation.

There are few studies employed RANSE method to evaluate the effects of roughness and biofouling on marine propeller performance, and total ship resistance such as: Suga et al. [4], Apsley et al. [5], Aupoix et al. [6], Eça et al. [7]. Those studies indicated that applying wall-functions can simulate the impact of uniform roughness on the skin resistance component of flat plates with high accuracy. Khor and Xiao [8] have conducted a study of the influence of fouling on the ship resistance by RANSE method. They applied the wall-function to take into account the uniform sand-grain function model. However,

Manuscript received May 31, 2021; revised October 23, 2021.
Corresponding author: Vu Ngoc Bich

doi: 10.18178/ijmerr.11.1.15-21

according to ITTC [9], using the sand grain roughness function have disadvantage. Thus, it is necessary to develop new methods to solve this problem.
The aim of this study is to resolve this problem by applying a modified wall-function in Star-CCM+ software package to evaluate the effects of roughness and biofouling on the propeller characteristics. The proposed model's main advantage is it can evaluate the effect of fouling on the torque and thrust of the ship propeller by a simple roughness length scale (similar to Demirel et al.'s approach [10]).

This article is organized as follows: Section 1 presents a governing equations and roughness functions. Section 2 shows the numerical simulation setup. Section 3 demonstrates the results of the numerical simulation, which including: the first step was to verify and validate the numerical simulation of the propeller in open water condition by comparing numerical obtained results with measure values at model scale for a benchmarking Potsdam Propeller. The second one, numerical model was modified to take into account impact of fouling on propeller performance in open water condition. The results then present the influence of fouling on torque, thrust coefficients, and efficiency of the propeller due to the change of advance coefficients.

II. Materials and Methods

A. Governing Equations

Consider an incompressible flow in Cartesian coordinates. The equations for continuity and momentum are defined by (1) and (2) [11]:

$$\frac{\partial(\rho \bar{u}_i)}{\partial x_i} = 0 \tag{1}$$

$$\rho\frac{\partial u_i}{\partial t} + \rho u_j\frac{\partial u_i}{\partial x_j} = -\frac{\partial p}{\partial x_i} + \frac{\partial \tau_{ij}}{\partial x_j} \tag{2}$$

In which, u_i and x_i present velocity and position vectors, p is pressure, t presents time, ρ is fluid density and the stress tenser t_{ij} is calculated by

$$t_{ij} = 2\mu S_{ij} \tag{3}$$

$$S_{ij} = \frac{1}{2}\left(\frac{\partial u_i}{\partial x_j} + \frac{\partial u_j}{\partial x_i}\right) \tag{4}$$

A turbulence model is applied to close (1) and (2). Where μ is viscosity and S_{ij} is the strain-rate tensor. $S_{ji} = S_{ij}$, so that $t_{ji} = t_{ij}$ for simple viscous fluids.

B. Turbulence Model

SST k-ω turbulence model was employed in this study as this proves to be able to predict the ship hydrodynamic accurately [12, 13].

Employing SST k-ω model, (1) and (2) are solved, and k and ω are determined by the equations below [14]:

$$\frac{d}{dt}\int_V \rho k dV + \int_A \rho k(u_i - u_{gi})da_i = \int_A \left(\mu + \frac{\mu_t}{\sigma_k}\right)\frac{\partial k}{\partial x_i}da_i + \int_V [\gamma_{eff} G_k - \gamma' \rho\beta^* f_{\beta^*}(\omega k - \omega_0 k_0) + S_k] dV \tag{5}$$

$$\frac{d}{dt}\int_V \rho\omega dV + \int_A \rho\omega(u_i - u_{gi})da_i = \int_A \left(\mu + \sigma_\omega \mu_t\right)\frac{\partial \omega}{\partial x_i}da_i + \int_V [G_\omega - \rho\beta(\omega^2 - \omega_0^2) + D_\omega + S_\omega] dV \tag{6}$$

Where: S_ω represents the user specified source term; ω_0 and k_0 present turbulence values in the source terms that counteracts turbulence decay; σ_ω and σ_ω present the inverse turbulent Schmidt number; f_c presents the correction factor of curvature; G_k and G_ω represent turbulent production terms; γ_{eff} presents the effective intermittency; D_ω presents the cross-derivate term; f_{β^*} presents the function used for free-shear; β and β^* represent model coefficients; γ' is defined by (5):

$$y' = \min[\max(\gamma_{eff}, 0.10,1] \tag{7}$$

$$\mu_t = \rho k T \tag{8}$$

Where: T is the turbulent time scale.

C. Wall-function Approach for Fouling Conditions

The roughness function model for fouling conditions is given by Eq. (7) as follows [14]:

$$\Delta U^+ = \begin{cases} 0 & \rightarrow k^+ < 3 \\ \frac{1}{k}\ln(0.26k^+)^{\sin\left[\frac{\pi}{2}\frac{\log(k^+/3)}{\log(5)}\right]} & \rightarrow 3 < k^+ < 15 \\ \frac{1}{k}\ln(0.26k^+) & \rightarrow 15 < k^+ \end{cases} \tag{9}$$

Where: k^+ presents roughness Reynolds number; ΔU^+ presents the roughness function; k presents the von Karman constant roughness function model has three flow regimes: smooth, a transitionally rough and a fully rough regimes.

III. Numerical Simulation

A. Propeller Test Case

In this paper, Potsdam propeller is selected as Propeller test case. This VP1304 propeller was designed in 1998. It is used to verify a numerical simulation results to experimental results. All the necessary data (geometrical parameters of propeller and experimental data in open water condition) of this propeller are provided in reference [15]. The geometrical parameters of Potsdam propeller are illustrated in Fig. 2 and Table I.

B. Modelling Method

There are three approaches for open water propeller simulation, that including [16]: Rotating Reference Frame

Method, Sliding Mesh Method and Whole fluid domain rotation method. In this study, Rotating Reference Frame Method is applied to investigate the impacts of fouling on propeller characteristic due to this method has big advantage in comparison with others in level of accuracy and computational time.

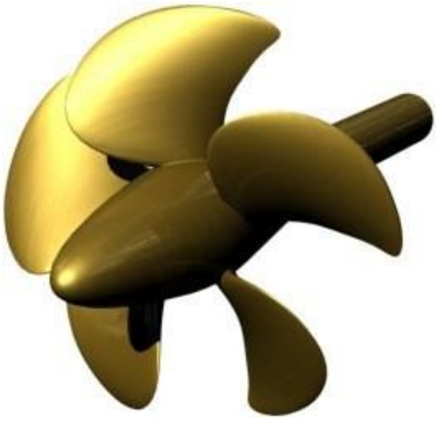

Figure 2. Potsdam propeller model.

TABLE I. POTSDAM PROPELLER PARAMETERS [15]

Propeller parameters	Symbol	Unit	Value
Diameter of propeller	D	m	0.25
Blade area ration of propeller	AE/A0	-	0.779
Pitch ration r/R=0.70	P0.7/D	-	1.635
Chord Length 0.7 (m)	C0.7	m	0.104
Skew angle	θ	Deg.	18.837
Hub ratio	Dh/D	-	0.3
Number of propeller blades	Z	-	5
Direction of rotation of propeller	-	-	Right
Propeller revolution	n	rps	15

C. Computational Domain, Boundary Conditions and Mesh Generation

One of the factors effect on numerical predicted results is selecting the size of computation domain, type of boundary conditions and mesh type and mesh generation concept. For Rotating Reference Frame Method, based on the recommendation of references [16] and [17], the computational domain is a cylinder with the following dimensions: The inlet boundary outlet boundary are located at a distance of 5D and 6D. The far field boundary is placed at a distance of 6D from the axis of propeller. For The boundary conditions, they were chosen as follows: No-slip wall condition is applied for propeller, the velocity inlet condition is used on inlet boundary, the pressure outlet condition is applied for outlet boundary, and symmetry plane condition is used on far field boundary (see Fig. 3).

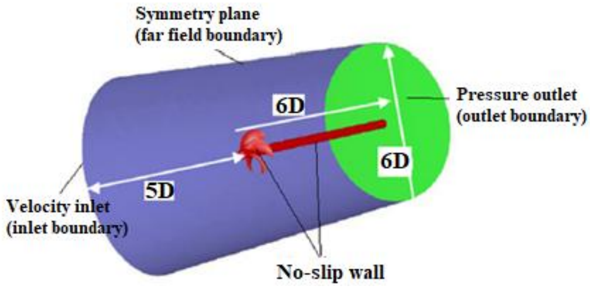

Figure 3. Computational domain and boundary conditions.

The mesh type employed in this study is hexahedral grid due to it provides better results than polyhedral grid [16]. The coarse grid was applied in the unimportant locations (the location far from propeller). For important regions including: propeller blades, shaft of propeller will be more refined due to it significant effects on numerical obtained results. The local refinement is applied near the propeller regions. To capture the flow near and around the walls, the prism layer was used to resolve the boundary layer. The result of mesh generation is displayed in Fig. 4.

IV. RESULTS AND DISCUSSIONS

A. Verification and Validation Study

It is sensible to choose the suitable grid size because its can effect on the numerical accuracy of obtained results. Thus, firstly, grid sensitivity study should be conducted in the manner of the ITTC procedure with the refinement ratio r_i equal to $\sqrt{2}$ [17]. In presented case, verification study for grid density is carried out at advance coefficient J=1.0 and roughness equal zero with three mesh: coarse, medium and fine mesh corresponding to the number of 1.42, 2.78 and 5.35 million cells, respectively.

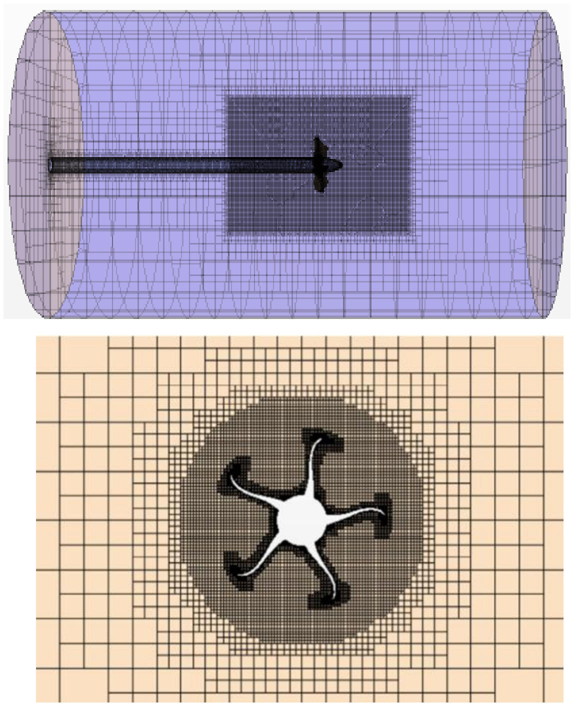

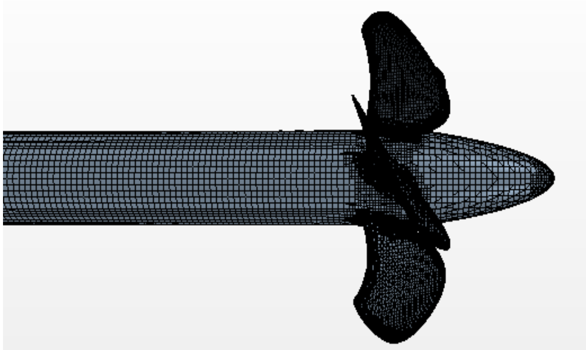

Figure 4. Result of grid generation.

Convergence ratio is determined as follows:

$$R_i = \frac{\varepsilon_{21}}{\varepsilon_{32}} \tag{10}$$

Where: S_1, S_2, S_3 present results achieved by using fine, medium, coarse grids, respectively; $\varepsilon_{21} = S_2 - S_1$ and $\varepsilon_{32} = S_3 - S_2$. There are three kinds of possible convergence conditions: oscillatory convergence ($R_i < 0$), divergence ($R_i > 1$), monotonic convergence ($0 < R_i < 1$).

The order of accuracy (p_i), correction factor (C_i) and the error (δ_{REi}) determined as follows:

$$p_i = \frac{\ln(\varepsilon_{32}/\varepsilon_{21})}{\ln(r_G)} \tag{11}$$

$$\delta_{RE_1} = \frac{\varepsilon_{21}}{r_G^{p_G} - 1} \tag{12}$$

$$C_i = \frac{r_G^{p_G} - 1}{r_G^{p_{iest}} - 1} \tag{13}$$

The uncorrected uncertainty (U_i) are determined as follows:

$$U_i = \begin{cases} [9.6(1-C_i)^2 + 1.1]\left|\delta_{RE_{i,1}}\right|, & |1-C_i| < 0.125 \\ [2|1-C_i| + 1]\left|\delta_{RE_{i,1}}\right|, & |1-C_i| \geq 0.125 \end{cases} \tag{14}$$

The uncertainty analysis results based on the grid dependency is given in Table II.

Table III illustrates the validation of the numerical result. In which E%D is the error of the numerical results of the medium grid case. A steady flow is adopted for the simulation, hence the time step uncertainty (U_T) and iterative errors (U_I) can be neglected in validating process. Hence, the numerical uncertainty is equal to grid uncertainty, it means that $U_{SN} = U_G$ [17]. The validation uncertainty is computed by the equation $U_V = \sqrt{U_G^2 + U_D^2}$. As the experimental uncertainty was not given in the reference study then the uncertainty of model test (U_D) is neglected. Thus, $U_V \cong U_G$.

TABLE II. THE UNCERTAINTY ANALYSIS RESULT BASED ON THE MESH DEPENDENCY AT J=1.0

Propeller characteristics		K_T	$10K_Q$
Computed values	S_1fine)	0.400	0.980
	S_2mid)	0.405	0.992
	S_3 (coarse)	0.429	1.010
Refinement ratio	$r_{21} = h_2/h_1$	1.414	1.414
Difference between solutions	$\varepsilon_{21} = S_2 - S_1$	1.426	1.426
	$\varepsilon_{32} = S_3 - S_2$	0.005	0.012
Convergence ratio	R_G	0.024	0.018
The error	δ_{RE}	0.208	0.667
Order of accuracy	p_G	0.001	0.024
Correction factor	C_G	4.53	1.17
Uncorrected uncertainty	U_G	3.8	0.5

Table III indicates that the error (the difference between the numerical result and the measured value) was smaller than validation uncertainty $|E|<U_V$ for K_T and K_Q. Therefore, the numerical simulation results were validated for propeller simulation, so the medium grid was applied in further studies.

TABLE III. VALIDATION OF THE NUMERICAL SIMULATIONS

Propeller characteristics	Symbol	E%D	U_V%D
Thrust coefficient	K_T	1.50	2.10
Torque coefficient	$10K_Q$	1.74	8.50

Table IV shows the comparison between calculated and measured characteristics of propeller in the case of smooth condition at all range of J. It can be seem in Table IV that good agreement between predicted and experimental results. The discrepancy between computed results and measured values was within 1.27% to 3.72% for K_T, 0.29% to 1.97% for K_Q and 0.67% to 5.86% for η_0 at all range of advance coefficient.

B. Effects of Biofouling on Propeller Characteristics

The impacts of different roughness conditions on propeller characteristics are invers gated in this section. Three case studies with different roughness conditions are demonstrates in Table V with the change characteristics of propeller due to different roughness surface conditions with respect to smooth condition (experimental results).

TABLE IV. NUMERICAL RESULTS OF OPEN WATER PROPELLER CHARACTERISTICS FOR SMOOTH CONDITION IN COMPARISON WITH MEASURED VALUE

J	***K_T***			***$10K_Q$***			***η_0***		
	EFD	***CFD***	***E%D***	***EFD***	***CFD***	***E%D***	***EFD***	***CFD***	***E%D***
0.60	0.6280	0.637	1.27	1.397	1.40	0.29	0.430	0.434	1.04
0.80	0.5100	0.520	1.96	1.179	1.19	1.02	0.552	0.556	0.98
1.00	0.400	0.405	1.50	0.976	0.992	1.74	0.653	0.650	0.34
1.20	0.2960	0.301	2.03	0.777	0.768	1.03	0.727	0.749	3.10
1.40	0.1870	0.195	3.72	0.560	0.548	1.97	0.750	0.793	5.86

As can be observed from Table V, Figs. 5, 6 and 7, the change in thrust coefficient (K_T) is higher than torque coefficient (K_Q). The obtained numerical results also demonstrate that tendency of reducing K_T and η_0 with increasing surface roughness. Besides, the Fig.7 shows that the higher advance coefficient (J) the larger the reduction in open water efficiency (η_0). The reduction in open water efficiency of 4.6% at J=0.6 and 22.9% at J=1.4 with the roughness ks=100 μm. The small calcareous fouling (ks=1000 μm) caused a reduction in the open water efficiency of 11.02% at J=0.6 and 53.25% at J=1.4

TABLE V. COMPARISON OF THE CALCULATED OPEN WATER CHARACTERISTICS WITH DIFFERENT ROUGHNESS CONDITIONS

J	*K_T*			*$10K_Q$*			*η_0*		
	CFD	*Smooth*	*% smooth*	*CFD*	*Smooth*	*% smooth*	*CFD*	*Smooth*	*% smooth*
				ks=100 μm (Deteriorated coating or light slime)					
0.6	0.610	0.637	4.24	1.420	1.400	1.43	0.410	0.43	4.60
0.8	0.491	0.520	5.58	1.192	1.190	0.17	0.524	0.551	4.82
1.0	0.366	0.405	9.63	0.969	0.982	-1.32	0.601	0.652	7.80
1.2	0.249	0.301	17.28	0.751	0.768	-2.21	0.633	0.726	12.78
1.4	0.134	0.195	31.28	0.517	0.548	-5.66	0.578	0.749	22.90
				ks=1000 μm (Small calcareous fouling or weed)					
0.6	0.585	0.637	8.160	1.46	1.400	4.29	0.383	0.43	11.02
0.8	0.4636	0.521	11.02	1.255	1.190	5.46	0.470	0.551	14.64
1.0	0.338	0.405	16.54	1.041	0.982	6.01	0.517	0.652	20.74
1.2	0.221	0.301	26.58	0.838	0.768	9.11	0.504	0.726	30.62
1.4	0.099	0.195	49.23	0.63	0.548	14.96	0.350	0.749	53.25

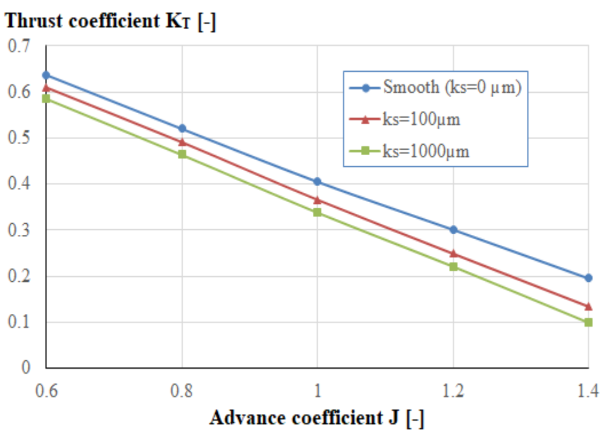

Figure 5. Thrust coefficient values for different roughness conditions.

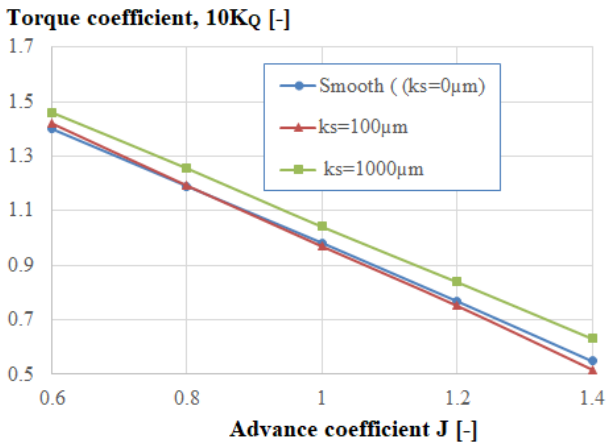

Figure 6. Torque coefficient values for different roughness conditions.

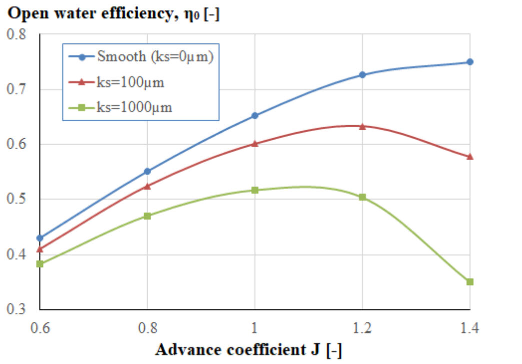

Figure 7. Open water efficiency values for different roughness conditions.

Fig. 8 and Fig. 9 show the distribution of skin friction coefficient and total pressure coefficient on blade of propeller at J=0 for different surface conditions, respectively. As can be observed from Fig. 8 and Fig. 9 that, the roughness rates significant effect on distribution skin friction coefficient on blade of propeller. As can be observed in the Fig. 8, Skin friction coefficient increases significantly with increasing the surface roughness. This observation is in agreement with the reduced shear thrust and increased shear torque coefficients components. The total pressure coefficient reduced with increasing the surface roughness, which is believed to be linked to reduce thrust and torque of propeller.

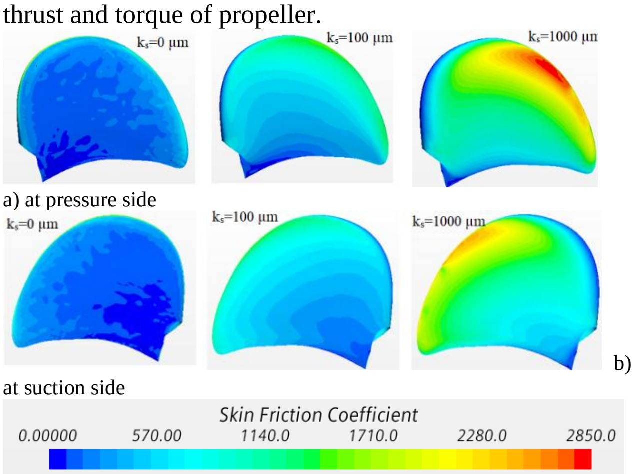

Figure 8. Distribution of Skin friction coefficient on blade of propeller at J=1.0

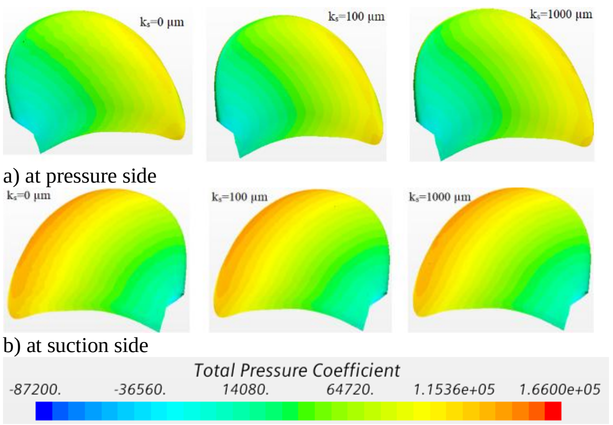

Figure 9. Distribution of total pressure coefficient on blade of propeller at J=1.0.

Fig. 10 illustrates the axial velocity on the $y = 0$ plane in smooth and fouled (ks=100 and 1000 μm) surface conditions at advance coefficient J=1.00. As can be seen in Fig. 10, the fouled cases show more scattered velocity distributions compare to the smooth case, which is believed to be linked to the pressure distribution resulting in thrust loss.

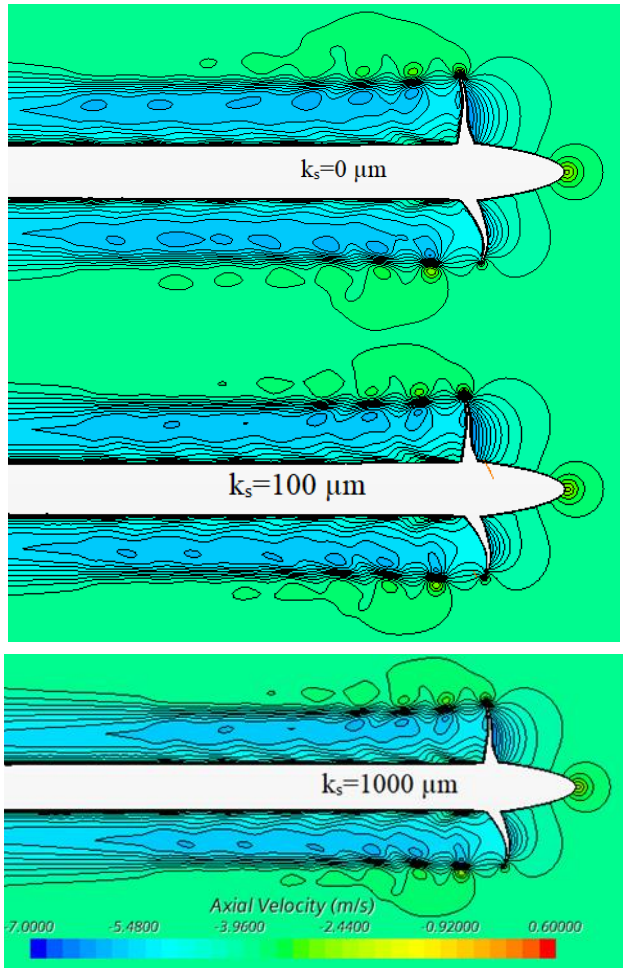

Figure 10. Distribution of axial velocity on the $y = 0$ plane in smooth and fouled surface conditions at J=1.0

V. Conclusion

In this article, a RANSE method for the evaluation of open water propeller performance has been presented using a benchmarking Potsdam Propeller. The moving reference frame method was applied to simulate the propeller model with different levels of roughness. A modified wall-function was applied to modelled roughness condition. The article reported good agreement between simulated results and experimental results.

Numerical obtained results indicated that with increasing level of roughness on the ship propeller surface, the magnitude of K_Q increases while the K_T decreases, that leads to the reduction in open water propeller efficiency of up to 53% at the highest simulated fouling rates. The decreases in the open water propeller efficiency were evaluated to be 4.6 % at J=0.6 and 22.9% at J=1.4 for a roughness ks=100 μm, 11.02% at J=0.6 and 53.25% at J=1.4 for a roughness ks=1000 μm. These indicated that the influence of fouling on ship propeller characteristic is significant and depend on fouling conditions and advance coefficients

CONFLICT OF INTEREST

The authors declare no conflict of interest.

AUTHOR CONTRIBUTIONS

Vu Ngoc Bich: Conceptualization, Methodology, Investigation, Visualization, Software, Resources, Supervision, Writing - revised draft, Writing - review & editing. Nguyen Thi Ngoc Hoa: Conceptualization, Methodology, Investigation, Writing - original draft, Writing - review & editing.

ACKNOWLEDGEMENT

The author is grateful to the Binh Duong University and Ho Chi Minh City University of Transport, Vietnam for providing all research facilities during executing this work.

REFERENCES

[1] M. P. Schultz, "Effects of coating roughness and biofouling on ship resistance and powering," *Biofouling*, vol. 23, no. 5, pp. 331-341, 2007.

[2] Y. K. Demirel, O. Turan, and A. Incecik, “Predicting the effect of biofouling on ship resistance using CFD,” *Journal of Applied Ocean Research*, vol. 62, pp. 100-118, 2017.

[3] *ITTC.* Specialist committee on surface treatment–final report and recommendations to the 26th ITTC. in *Proc. 26th ITTC–Volume II.*

[4] K. Suga, et al., “An analytical wall-function for turbulent flows and heat transfer over rough walls,” *International Journal of Heat and Fluid Flow*,. vol. 27, no. 5, pp. 852-866, 2006.

[5] D. J. F. Apsley, “Turbulence and combustion, CFD calculation of turbulent flow with arbitrary wall roughness,” *Flow, Turbulence and Combustion*, vol. 78, no. 2, pp. 153-175, 2007.

[6] B., Aupoix, “A general strategy to extend turbulence models to rough surfaces: Application to Smith’Sk-L model,” *Journal of Fluids Engineering*, p. 129 (10), 1245-1254, 2007.

[7] L. Eça, M. J. C. Hoekstra, “Numerical aspects of including wall roughness effects in the SST k–ω eddy-viscosity turbulence model,” *Computers & Fluids*, vol. 40, no. 1, pp. 299-314, 2011.

[8] Y. S. Khor and Q. J. O. E. Xiao, “CFD simulations of the effects of fouling and antifouling,” *Ocean Engineering*,. vol. 38, no. 10, pp. 1065-1079.

[9] *ITTC, 2011b. Practical Guidelines for Ship CFD Application, ITTC Recommended Procedures and Guidelines, Procedure 7.5-03-02-03, Revision 01.*

[10] Y. K., Demirel, et al., “A CFD model for the frictional resistance prediction of antifouling coatings,” *Ocean Engineering*, vol. 89, pp. 21-31, 2014.

[11] D. Wilcox, *Turbulence Modeling for CFD,* 2006.

[12] Z. Yong, et al., “Turbulence model investigations on the boundary layer flow with adverse pressure gradients,” *Journal of Marine Science and Application,* vol. 14, no. 2, pp. 170-174, 2015.

[13] L. Larsson, F. Stern, and M. Visonneau, *Numerical Ship Hydrodynamics: An Assessment of the Gothenburg 2010 Workshop*, 2013: Springer.

[14] *Siemens, 2020. STAR-CCM+ User Guide.*

[15] U. Barkmann, H. J. Heinke, and L. Lübke, “Potsdam propeller test case (PPTC),” in *Proc. the Second International Symposium on Marine Propulsorssmp’11*. 2011.

[16] T. N., Tu, *Numerical Simulation of Propeller Open Water Characteristics Using RANSE Method,* Alexandria Engineering Journal, vol. 58, no. 2, pp. 531-537, 2019.

[17] *ITTC – Recommended Procedures and Guidelines. Practical Guidelines for Ship Self-Propulsion CFD. 2014.*

Vu Ngoc Bich was born in 1961. Graduated with a PhD (2007) in Russia. Associate professor in 2013.
He is currently a Senior Lecturer, Institute of Industrial Management and Logistics, Binh Duong University. His current interests include the design and optimization of ships and transportation equipment.

Nguyen Thi Ngoc Hoa received her Bachelor degree (2002) and M.Sc. degree (2013) from Ho Chi Minh city University of Transport.
She is a Lecturer, Institute of Mechanical Engineering, Ho Chi Minh city University of Transport. Her current interests include ship design, stability and optimization.